Nuclear Instruments and Methods in Physics Research A300 (1991) 179–187
North-Holland

Shielding properties of iron at high energy proton accelerators studied by a Monte Carlo code

K. Tesch and J.M. Zazula [1]

Deutsches Elektronen-Synchrotron DESY, Notkestrasse 85, W-2000 Hamburg 52, Germany

Received 21 May 1990 and in revised form 31 August 1990

Shielding properties of a lateral iron shield and of iron and concrete shields at angles between 5° and 30° are studied by means of the Monte Carlo program FLUNEV (DESY-D3 version of the FLUKA code extended for emission and transport of low energy neutrons) The following quantities were calculated for a high energy proton beam hitting an extended iron target: total and partial dose equivalents, attenuation coefficients, neutron spectra, star densities (compared also with the CASIM code) and quality factors The dependence of the dose equivalent on the energy of primary protons, the effect of a concrete layer behind a lateral iron shielding and the total number of neutrons produced in the target were also estimated.

1. Introduction

In our previous article [1] we reported irradiation protection quantities of interest (dose equivalent and absorbed doses in tissue, particle currents and spectra emerging from a shield, mean quality factors, attenuation lengths) calculated by the Monte Carlo code FLUNEV [9] for lateral ordinary concrete and heavy concrete shields. The source was a thick iron target irradiated by a high energy (25–800 GeV) proton beam. The aim of the following report is to consider iron as another shielding material used at proton accelerators.

It is well known that iron is a shielding material not as favorable as concrete because of its relatively high transparency for neutrons below 1 MeV. This is due to the smaller total cross sections in the lower keV range, to smaller lethargy changes and stronger forward peaking in elastic scattering and to the absence of significant neutron capture reactions. A strong buildup of low energy neutrons is expected in an iron shield of practical dimensions, with no radiation equilibrium between high and low energy components of secondary radiation, making their attenuation lengths dependent on shield thickness, energy range and angle. On the other hand, iron is an excellent shielding material against high energy hadrons and leptons because of its high density, large inelastic interaction cross section, low production of secondary particles relative to heavier elements, and its moderate price. By inelastic scattering iron effectively reduces neutron energies down to 1 MeV. Therefore iron shields (with or without additional concrete) are in use around experiments at accelerators; sometimes magnets of an experiment have an additional shielding purpose. The present investigation was stimulated by the question how far the two detectors at the electron-proton storage ring HERA at DESY can be regarded as self-shielding devices.

For dimensioning iron shields only very little information can be found in the literature. Deep penetration calculations in iron are considered as especially difficult, time consuming and being sensitive to input data. For protection purpose, and contrary to the case of a concrete shield, secondary neutrons should be followed down to at least 10 keV in the total system. Simple parametrization formulas to calculate the dose equivalent as a function of the shield thickness are not at hand, or they have no clear physical interpretation. Attenuation coefficients to be expected in iron for some geometries and some energy ranges are compiled in ref. [4]. Calculations for the simplest geometry of a large proton absorber (backstop geometry) are discussed by Thomas and Stevenson [5]. Measurements of neutron fluences above 20 MeV are reported by Bennett et al. [6].

Our calculations for the proton absorber case had been discussed and compared to experimental data [8] in the recent report [2]. In course of the current study, we calculated radiological quantities behind lateral iron shields and at small angles to the beam direction behind a combination of iron of different thicknesses and ordinary concrete. The layout of considered geometries is described in the next section of this report together

[1] On leave of absence from the Institute of Nuclear Physics, Krakow, Poland.

0168-9002/91/$03.50

with other details of the calculations. The results are given in section 3. Normalized and smoothed current spectra and dose equivalent spectra for neutrons emerging from different shields have been included in the appendix of our DESY report [3].

2. Comments on the calculational method and description of geometrical models

The calculations were performed by using the Monte Carlo program FLUNEV [9], our extension of the hadronic shower code FLUKA87 [10] developed at CERN, which includes production and transport of secondary neutrons below 50 MeV. FLUNEV is linking into one program the high energy event generator and transport module of FLUKA, the evaporation module EVAP-5 (taken from the HETC/KFA code [11]), and a low energy neutron transport module. The latter is based on the FLUKA geometry packages, the neutron collision and cross section package extracted from the neutron transport code MORSE (ORNL) [12], and the cross section library HILO86 [13] supplemented by kerma factors [14,15] and dose conversion factors [16]. The library contains differential neutron cross sections in multigroup approximation and Legendre expansion up to P_5 which is at least necessary for studying neutron transport in iron.

In the most recent report [2] we verified the FLUNEV model applied to interactions of energetic protons and their secondaries with iron by comparison with data measured around thin iron targets and a thick iron absorber. We especially mentioned some modifications in calculating the intranuclear cascade energies and nuclear excitation energies. For other features of the FLUNEV code and of the coupled programs and for further details concerning the theoretical models and the cross sections, kerma factors and conversion factors applied to calculate dose equivalents and other magnitudes of radiological interest the reader is referred to the FLUNEV description [9], to the documentation of the relating codes and data sets [9–16], and to our previous reports [1,2].

In order to save computing time collisions and transport of secondary neutrons were simulated down to thermal energy group (below 0.4 eV) only in the last 50 cm before an external shield boundary and in the following layer of the tissue-equivalent material. In the target the energy cutoff for neutron transport was 1 MeV (except of the runs with no shield and with shields thinner than 40 cm of iron). This energy is low enough since the dose outside the shield is dominated by low energy neutrons produced in the shield by neutrons of much higher energies. In other regions neutron histories were terminated and their energy assumed to be absorbed within one inelastic interaction length after slowing down below 10 keV; this limit is below the energy range of smallest total cross section (around 25 keV). All jobs were submitted on an IBM 3084 computer with calculation times varying from 20 min (0 cm of iron shield) to 70 min (140 cm and more).

As in the reference report [1], we calculated the dose equivalent outside the shield by two different methods in order to check and understand the results. First the dose equivalent is obtained by multiplying the particle one-way current (mostly neutron current) emerging from the shield boundary by conversion coefficients, second we calculated the absorbed dose in a suitable phantom and multiplied it by quality factors. For the use of quantities like fluence, current and conversion factors, and for the data sources we refer also to the detailed discussion in our earlier paper [1]. All conversion coefficients for neutrons refer to the case of a broad parallel neutron beam impinging either on a 30 cm tissue sphere (e.g., for calculations of the ambient dose equivalent $H(10)$ at depth of 10 mm in an aligned field) or on a tissue slab (perpendicular incidence; note the same value of current and fluence quantities for that case). Therefore their use can only be an approximation for our actual case; multiplication with the neutron current (number of neutrons per unit area of traversed shield boundary) instead of neutron fluence (number of neutrons per unit area traversing the boundary, divided by the cosine of their respective angle between flight direction and normal of the boundary) means that we just assume the perpendicular incidence; angular-dependent conversion factors are not available, the angular distribution of neutron leakage is not accounted for by us. Since the dose outside a shield, especially outside a lateral shield, is mainly due to low energy neutrons, this approximation is quite good: the dose attenuation factors in a 30 cm slab of tissue for neutrons with energies of 14, 5 and 1.5 MeV are 5, 10 and 100, respectively [19]; this means that most of the dose is deposited within the first few centimeters of tissue and that it is approximately independent of the angle of incidence. For the mentioned second method of dose equivalent calculation we had to calculate the absorbed dose average over not more than the first 2 cm layer of the lateral tissue (the rest acting as a backscatterer) in order to get good agreement (within 10%) between both methods. Larger differences were only found for neutrons below 20 keV; probably the used data sets of kerma factors, quality factors and conversion factors are not consistent in this energy range.

The shielded object was a thick iron target irradiated by a high energy (50–800 GeV) proton beam. Two cases were considered: shielding at transverse directions (around 90°) and shielding at small angles (5°–30°); the respective cylindrical geometry models are shown in fig. 1. Some changes of this basic layout to receive specific results are discussed in the next section. The

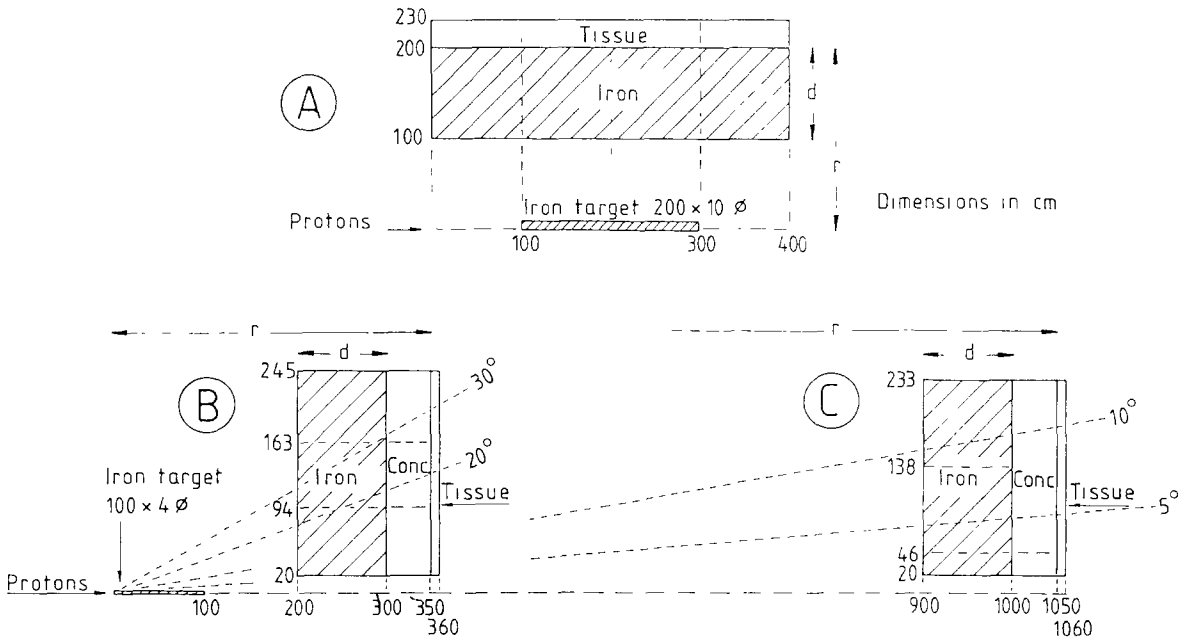

Fig. 1. Geometrical models used in the Monte Carlo calculations. The upper drawing (A) represents the case of lateral shielding, the drawings below (B and C) are the geometries for shielding at forward directions (at 5–10° and 20–30°). An iron thickness of 100 cm is shown as an example.

thickness d of the lateral shield varied between 0 and 180 cm; at forward angles we studied iron shields between 50 and 150 cm only in combination with an additional concrete layer of fixed thickness (50 cm). We did not study a shielding in beam direction (at 0°); this case is seldom realized at very high energies, and behind a compact iron or concrete shield the dose is due to penetrating muons, a component whose calculation is out of the scope of this work. A cylindrical layer of 30 cm tissue was the phantom in which doses were calculated for transverse directions; at small angles the tissue layer of 10 cm thickness was assumed to be sufficient. The density of iron is 7.88 g/cm^3; densities and isotopic compositions of other materials are the same as given in table 4 of the previous report [1].

3. Discussion of results

3.1. Total and partial dose equivalents

The total dose equivalents and the dose equivalents of several radiation components were calculated for

Table 1
Magnitudes of the total dose equivalent H_{tot} per one 100 GeV proton and relative contributions of neutrons in four energy ranges, behind lateral iron shields of different thicknesses d; the geometry is described in fig. 1a

Fe shield d [cm]	$H_{tot} \times 10^{-14}$ [Sv]	Neutron contribution to H_{tot} [%]			
		$E > 50$ MeV	50–2 MeV	2–0.02 MeV	$E < 20$ keV
0	82.0	7.7	35	57	0.3
20	32.0	5.4	18	74	1.0
40	13.0	3.8	8.7	86	1.7
60	4.50	2.0	6.1	90	2.6
80	1.60	2.3	4.3	91	2.8
100	0.50	1.7	5.2	90	3.8
120	0.17	3.8	2 2	90	3.9
140	0.054	2.2	1.3	93	3.9
160	0 018				
180	0.005				

transverse directions and for small angles. The proton beam energy was 100 GeV.

The lateral iron shield was varied between 0 and 180 cm, in each case only the results concerning the maximum dose are presented which occurs roughly at an angle of 70° (seen from the maximum of energy deposition in the target). The size of the iron target was 200 cm length × 10 cm diameter. The lateral dose is almost entirely due to neutrons, behind an iron thickness of only 40 cm the contribution of protons and pions is less than 1%. Table 1 shows the total dose equivalent H_{tot} as a function of iron thickness and the contributions of four neutron energy ranges. With a thickness larger than 40 cm the dose is mostly produced by neutrons with energies between 2 MeV and 20 keV.

At angles of 5°, 10°, 20° and 30° we studied the dependence of dose on iron thickness only with an additional concrete layer of 50 cm behind the iron since such a shield is of greater practical interest than a pure iron shield. At these angles a greater influence of the target size is expected. We varied the length of the target between 30 and 200 cm and its diameter between 4 and 10 cm. The results in table 2 refer to an iron target 100 cm length × 4 cm diameter; the other target sizes give smaller doses in most cases but not smaller than by a factor of 3. The dose components are completely different from those at large angles, as expected; the contributions of the electromagnetic cascade and of charged hadrons is remarkable.

3.2. Attenuation coefficients

In an attempt to describe the attenuation in iron in a possibly simple way we deduced attenuation coefficients λ for the currents of high energy neutrons and of charged hadrons, at angles θ of 5°, 10°, 20° and 30°. For transverse directions we repeated calculations with a target of reduced length (30 cm) as a "pointlike" target, magnitudes of interest were taken at an angle of about 70°. In addition we calculated the star density S (number of inelastic interactions per cm^3, averaged over the last 10 cm of iron) and its attenuation coefficient. The effective thickness $d_{eff} = d/\sin\theta$ and the effective distance $r_{eff} = r/\sin\theta$ were taken into account for the lateral case, and $d/\cos\theta$ and $r/\cos\theta$ for the small angles geometry (see fig. 1 for the meaning of d and r). After separating a $1/r_{eff}^2$ dependence the assumption of an exponential decrease turned out to be good in all cases (the regression coefficients were between 0.97 and 1.00), and the resulting coefficients are displayed in table 3 as a function of angle, together with the λ of the total dose equivalent.

The strong dependence on angle is apparent in all cases. It is much stronger than expected for any isolated radiation component emerging from a target; especially the attenuation of star-producing particles and of neutrons above 50 MeV seems to be too high and not in agreement with the known inelastic cross sections. The reason is that the hadronic cascade developed in the target continues in the shielding material, there is no

Table 3
Attenuation coefficients in iron for the currents of all star-producing particles, charged hadrons, and neutrons with energies above 50 MeV, as a function of angle against the beam direction; also shown is the angular dependence of attenuation of the total dose equivalent, H_{tot}

Angle	λ [g/cm^2]			
	Stars	p, $\pi^\pm$	n (E > 50 MeV)	H_{tot}
5°	300	200	280	240
10°	240	160	220	190
20°	220		240	240
30°	210		180	200
45°	210			
≃ 70°			140	180
≃ 90°	140			

Table 2
Total dose equivalent H_{tot} per one 100 GeV proton, together with relative contributions of the electromagnetic cascade, charged hadrons and neutrons in two energy ranges, at two angles, behind forward iron shields of different thicknesses d and an additional concrete layer of 50 cm thickness; the geometry is described in fig. 1b and 1c

Fe shield d [cm]	Angle 5°					Angle 20°				
	H_{tot} ×10^{-14} [Sv]	Contribution [%]				H_{tot} ×10^{-14} [Sv]	Contribution [%]			
		EM casc.	p, $\pi^\pm$	n (E > 20 MeV)	n (E < 20 MeV)		EM casc	p, $\pi^\pm$	n (E > 20 MeV)	n (E < 20 MeV)
50	4 5	14	36	32	18	1.8	8	12	51	29
75	2 0	14	30	37	20	0.54	5	8	55	33
100	0 81	11	24	43	21	0.17	4	6	51	39
125	0 33	12	23	45	20	0.09	8	3	52	36
150	0 14	11	17	43	28	0 03	10	0	41	44
175	0.06	8	17	45	30					

radiation equilibrium between the different components, and the whole process is too complicated to be described by simple exponential terms with coefficients of understandable physical meaning. This is the same conclusion which we received in an earlier paper about concrete shielding [18]. An additional difficulty arises when the results from the three chosen geometrical models A, B and C (fig. 1) are compared with each other; a closer inspection of the results for low energy neutrons shows that the total dose behind the shield at the indicated angles and its attenuation in the shield is influenced by low energy neutrons produced in the shield region nearest to the primary beam line (at $r = 20$ cm).

Therefore the attempt of a simple description of the attenuation in iron in terms of physical quantities is

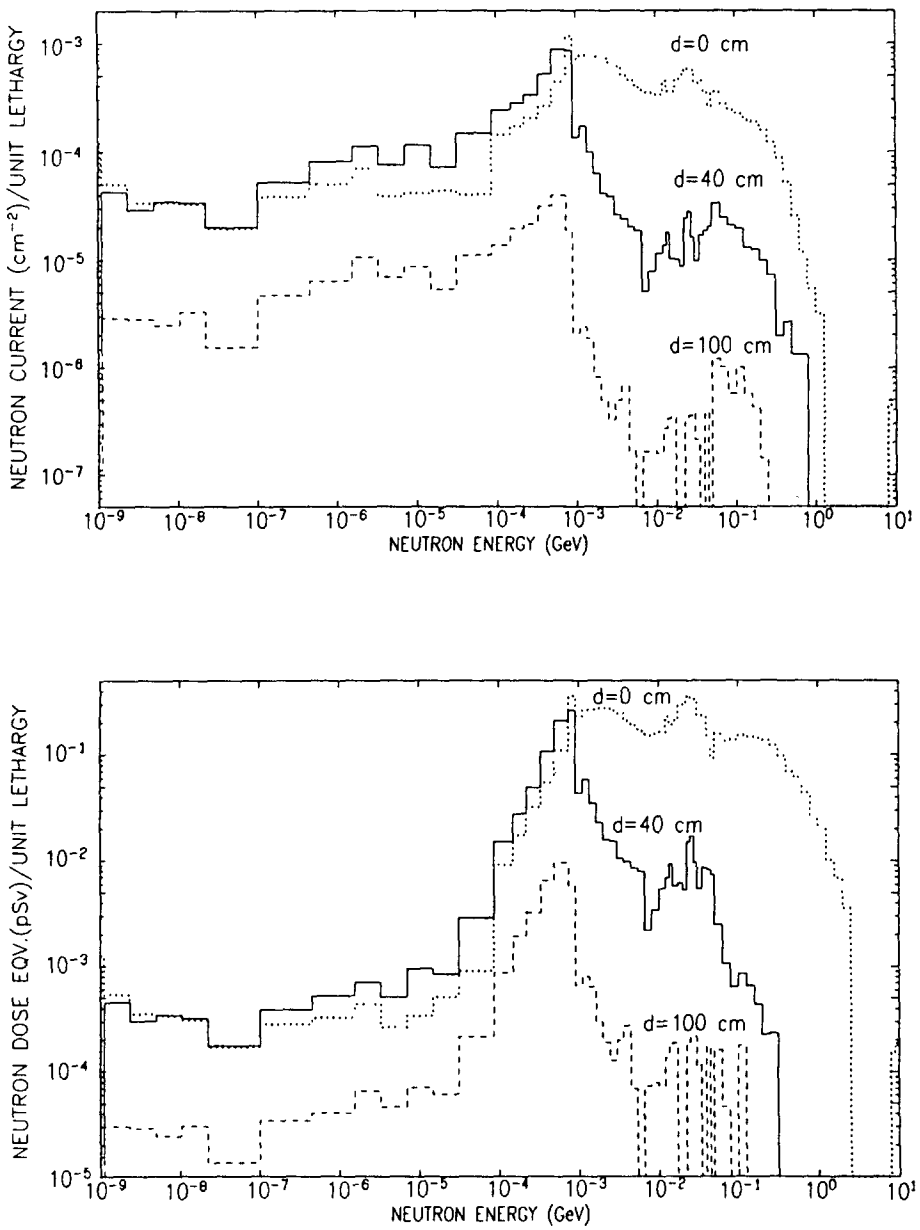

Fig. 2. Neutron current (upper plot) and neutron dose equivalent (lower plot) per one 100 GeV proton and per unit logarithmic energy decrement, behind a lateral iron shield of thickness d, as a function of neutron energy.

abandoned, and for practical purpose only it is reasonable to parametrize the total dose equivalent per one proton of energy E_p (in GeV) as

$$H_{tot} = H_0 E_p^{0.8} \frac{e^{-d/\lambda}}{r^2}. \quad (1)$$

For the sake of simplicity, the thickness d and distance r (in m) are taken here perpendicular to the primary beam for the lateral shield and parallel for the smaller angles; in the latter case the origin of r is the front face of the target. H_{tot} is the maximum of the total dose equivalent along the iron shield for the lateral case; for small angles it is the H_{tot} behind an iron shield of thickness d and an additional concrete layer of 50 cm, as above. For the targets see fig. 1, for the dependence on the primary energy E_p see section 3.4. The received

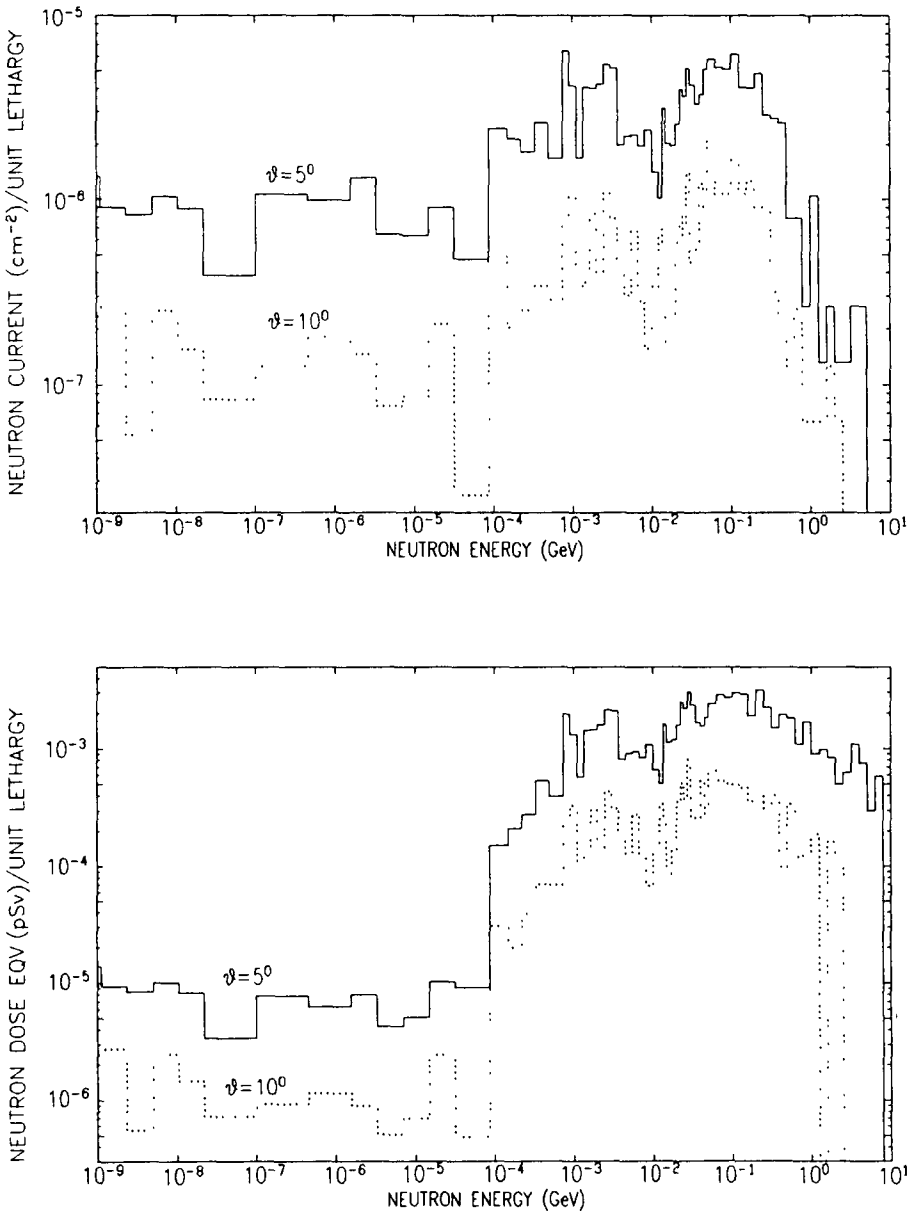

Fig. 3. Neutron current (upper plot) and neutron dose equivalent (lower plot) per one 100 GeV proton and per unit logarithmic energy decrement, at angles of 5° and 10° behind a forward shield of 100 cm iron and 50 cm concrete, as a function of neutron energy.

Table 4
Parameters of eq (1)

Angle	H_0 [Sv m^2]	λ [g/cm^2]	Considered range of iron thickness [cm]
5°	6.0-13 [a]	240	50–175
10°	2.2-13	190	50–175
20°	2.0-14	230	50–150
30°	6.6-15	170	50–150
≈ 70°	4.0-14	180	20–180

[a] Read as 6.0×10^{-13}

parameters H_0 and λ are shown in table 4. They strictly refer to the geometries displayed in fig. 1 and are not recommended for use in other case.

3.3. Neutron spectra

For practical purposes, e.g. for selecting suitable instruments and methods for neutron dosimetry, it is useful to know the neutron spectrum expected behind a shield. We present typical neutron spectra in figs. 2 and 3, normalized to one 100 GeV proton and for the targets indicated in fig. 1. For the case of lateral shielding the spectra for three iron thicknesses are taken at the dose maximum around 70°, the spectra at 5° and 10° are behind 100 cm iron and 50 cm of concrete. The drastic difference in the shapes of spectra is clearly seen; whereas at forward angles most of the dose equivalent is due to neutrons between 1 MeV and 1 GeV, the dose behind a lateral iron shield is produced by neutrons between 1 and 0.1 MeV.

Neutron current spectra and dose equivalent spectra, somewhat smoothed and normalized to 1 n/cm^2 and 1 pSv, respectively, are given in tabular form in the appendix of our DESY report [3], also for shielding materials other than iron for comparison; they are available on request.

3.4. Dependence on primary energy

It is already known that behind lateral shielding the dose increases slower than linearly with the energy of the primary beam. The $E_p^{0.8}$ dependence was first observed by Thomas and Thomas [7]. In the course of the present work we checked the E_p dependence also for forward angles. For energies between 50 and 800 GeV and from angles from 5° to 30° we found an E_p^x dependence with x between 0.75 and 0.79, practically the same relationship as at transverse directions.

The reason of this power law is the increasing dominance of the electromagnetic cascade. In the energy range mentioned above the energy deposited by this component in the iron target increases from 12.9 GeV (26%) at 50 GeV to 344 GeV (43%) at 800 GeV which gives a power law with $x = 1.19$ (regression coefficient of the fit is 0.99); in the total system this energy increases with $x = 1.09$. Since the neutron production by the electromagnetic cascade is very small as com-

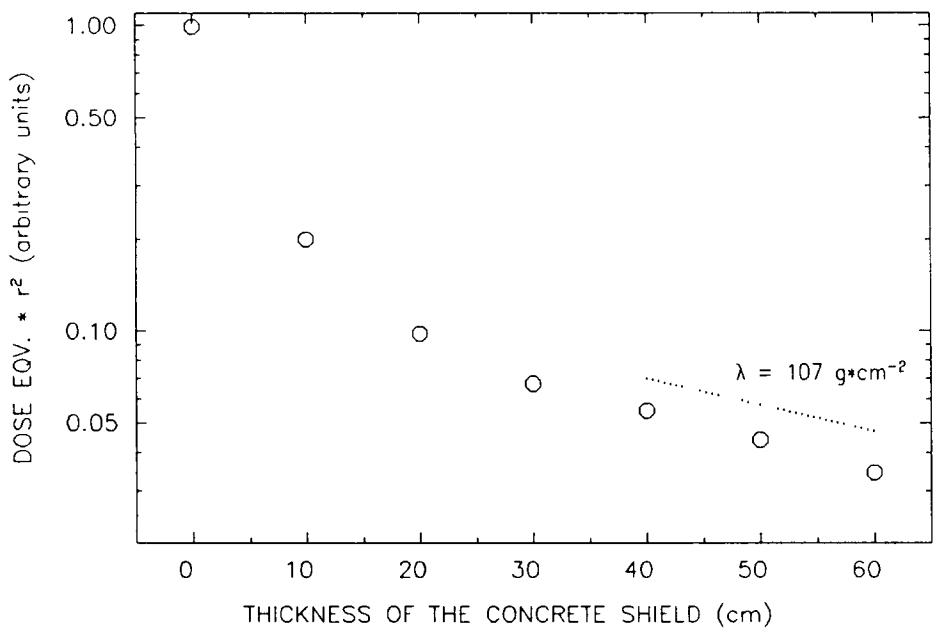

Fig. 4 Reduction of the dose equivalent behind a lateral iron shield of 40 cm thickness by an additional concrete shield. The attenuation in a pure concrete shield is indicated by λ

pared with that of the hadronic cascade, the increase of the neutron dose with energy is correspondingly slower.

3.5. Effect of a concrete layer added to a lateral iron shield

A pure iron shield at transverse direction is rather unsatisfactory, and from fig. 2 it is clear that addition of concrete will greatly reduce the dose. We calculated this effect quantitatively for an iron shielding of 40 cm and the lateral geometry of fig. 1, with additional concrete between the iron and tissue layer varying from 10 to 60 cm (in steps of 10 cm). After removing the purely geometrical attenuation the reduction in dose equivalent is shown in fig. 4. The neutrons below 1 MeV are absorbed by 20 cm of concrete, then the attenuation is reduced correspondingly to the attenuation coefficient 107 g/cm^2 received for concrete shielding [1,4].

3.6. Effective quality factors

Effective quality factors were calculated by dividing the dose equivalent (boundary crossing estimation) by the dose absorbed in the tissue phantom. They range from 3 to 4 at angles of 5° and 10° (geometry C, fig. 1) and from 4 to 6 at 20° and 30° (geometry B). This increase is explained by the increasing contribution of neutrons below 100 MeV. Behind lateral iron thicker than 20 cm the quality factor is 11.5, which is reduced to 6.7 by additional concrete, in agreement with the value for pure concrete shielding [1,4].

3.7. Thicker iron shields

It is not possible to get statistically significant results in a reasonable computing time for the geometries under discussion and for an iron shield thicker than about 1.5 m. For a rough estimate of dose equivalents behind thicker iron shields one can use the fast-running Monte Carlo program CASIM [17]. This program simplifies the physics of interactions drastically and is able to calculate energy densities and star densities in a very thick absorber; however, since the leading particle biasing is used in CASIM, it tends to overestimate the forward spread of hadronic cascades, relatively to transverse distribution. The star density S can be approximately correlated with the dose equivalent H by the simple expression $H = k_1 S$. For a lateral concrete shield a k_1 value of 4.4×10^{-8} Sv cm^3 was found [4], independent of other parameters like beam energy, target size and material or thickness of concrete.

In order to establish k_1 factors also for iron shielding we calculated star densities produced by particles with energies above $\simeq$ 50 MeV for the same geometries as above by using the CASIM code (and by means of FLUNEV, for comparison) at beam energy of 100 GeV. For the lateral shield (fig. 1A) S was averaged longitudinally over z = 200–300 cm and radially over the outer

Table 5
Total dose equivalents, star densities and k_1 factors versus geometry model, shield thickness and angle

Shielding geometry	Angle	Iron thickness [cm]	Dose equivalent [Sv]	Star density [cm^{-3}]		k_1 factor [Sv cm^3]
				FLUNEV	CASIM	
Forward (fig. 1c)	5°	50	4.6-14	1.9-06	2.7-06	1.7-08
		100	8.1-15	4.9-07	7.8-07	1.0-08
		150	1.4-15	9.1-08	1.6-07	8.9-09
		200	2.5-16	–	4.6-08	5.4-09
	10°	50	1.1-14	4.6-07	8.2-07	1.3-08
		100	1.3-15	9.7-08	1.9-07	6.6-09
		150	1.4-16	1.3-08	3.0-08	4.5-09
		200	1.7-17	–	8.4-09	2.0-09
Forward (fig. 1b)	20°	50	1.4-15	9.7-07	1.3-06	1.1-09
		100	2.4-16	1.5-07	2.0-07	1.2-09
		150	3.9-17	2.4-08	3.7-08	1.1-09
		200	6.4-18	–	1.2-08	5.3-10
	30°	50	2.6-16	2.0-07	1.7-07	1.5-09
		100	2.3-17	8.8-09	1.9-08	1.2-09
		150	2.1-18	–	2.8-09	7.5-10
		200	1.9-19	–	4.3-10	4.4-10
Lateral (fig. 1a)	$\simeq$ 70°	80	1.5-14	1.4-07	8.3-08	1.8-07
		160	2.1-16	4.1-10	3.4-10	6.4-07
		240	3.8-18	–	2.5-12	1.5-06

10 cm of iron; at smaller angles (fig. 1b and 1c) S was averaged over an outer concrete layer of about 15 cm. The S values are presented in table 5, together with the dose equivalent from eq. (1) and the resulting k_1 factors. These factors show a smooth behavior as a function of iron thickness for all three geometries, so they could be extrapolated and used also for deeper iron shields which are not accessible by means of the FLUNEV code. In contrast to the case of a lateral concrete shield, they increase with increasing thickness of the lateral iron shield due to the transport of low energy neutrons.

3.8. Neutron production from an unshielded target

Finally we give some information about the number of neutrons produced in an iron target. Occasionally this number is required in connection with experimental areas without roof, e.g. to estimate skyshine phenomena. We calculated the number of neutrons escaping the target; neutrons which leave the target at angles smaller than 20° and albedo neutrons (with backward directions) were neglected. The target was 2 m long, the diameter varied between 4 and 50 cm. For neutrons with energies above 2 MeV a maximum of 180 neutrons per one 100 GeV proton was obtained with a diameter of about 10 cm, this value dropped to 40 with a 50 cm target. For all neutrons (independent of energy) the number increased monotonically with target diameter from 220 to 720 per 100 GeV proton.

References

[1] J.M. Zazula and K. Tesch, DESY rep. 89-064 (1989); Nucl. Instr. and Meth. A286 (1990) 279.
[2] J.M. Zazula and K. Tesch, this issue, Nucl. Instr. and Meth. A300 (1991) 164.
[3] K. Tesch and J.M. Zazula, DESY rep. 90-037 (1990).
[4] K. Tesch and H. Dinter, Radiat. Protection Dosim. 15 (1986) 89.
[5] R.H. Thomas and G.R. Stevenson, IAEA Technical Report Series, no. 283 (Vienna, 1988)
[6] G.W. Bennett, G.S.Levine, H.W. Foelsche and T.E. Toohing, Nucl. Instr. and Meth. 118 (1974) 149.
[7] R.H. Thomas and S.V. Thomas, Health Phys. 46 (1984) 954.
[8] J.S. Russ, G.R. Stevenson, A. Fasso, M.C. Nielsen, C. Furetta, P.G. Rancoita and I. Vismara, CERN Divis. rep. TIS-RP/89-02 (1989).
[9] J.M. Zazula, int. rep. DESY-D3-66 (1990).
[10] P.A. Arnio, J. Lindgren, J. Ranft, A. Fasso and G.R. Stevenson, CERN Divis. reps. TIS-RP/168 (1986) and TIS-RP/190 (1987).
[11] P.Cloth, D. Filges, G. Sterzenbach, T.W. Armstrong and B.L. Colborn, KFA Jülich rep. Jül-Spez-196 (1983).
[12] M.B. Emmet, Oak Ridge National Laboratory rep. ORNL-4972 (1975).
[13] R.G. Alsmiller, Jr., J.M. Barnes and J.D. Drischler, Nucl. Instr. and Meth. A249 (1986) 445.
[14] M.A. Abdou, C.W. Maynard and R.Q. Wright, Oak Ridge National Laboratory rep. ORNL/TM-3994 (1973).
[15] J.M. Zazula, P. Cloth, D. Filges and G. Sterzenbach, Nucl. Instr. and Meth. B16 (1986) 506.
[16] G.R. Stevenson, CERN Divis. rep. TIS-RP/173 (1986).
[17] A. Van Ginneken, Fermi National Accelerator Laboratory rep. FN-272 (1975).
[18] H. Dinter, K. Tesch and C. Yamaguchi, Nucl. Instr. and Meth. A276 (1989) 1.
[19] J.A. Auxier, W.S. Snyder and T.D. Jones, in: Radiation Dosimetry, vol. 1, eds. F.H. Attix and W.C. Roesch (Academic Press, 1968).
[20] K. Morstin, B. Kawecka and J. Booz, 5th Symp. on Neutron Dosimetry, Munich/Neuherberg (1984).